Ecography

E7753

Eppinga, M. B., Pucko, C. A., Baudena, M., Beckage, B. and Molofsky, J. 2012. A new method to infer vegetation boundary movement from 'snapshot' data. – Ecography 000: 000–000.

Supplementary material

Appendix 1: Definition of the optimal vegetation boundary position

In this Appendix, we provide a more formal definition and description of the optimal vegetation boundary position, expanding on the definition and illustration (Fig. 1) provided in the main text. Consider a lattice of width L_X and length L_Y, with a total of $L_X * L_Y = Z$ elements, which is occupied by two vegetation communities, C_1 and C_2 that form a vegetation boundary. At time t, global densities of C_1 and C_2 are given by $\rho_1(t)$ and $\rho_2(t)$. In case that there are no unoccupied cells (e.g. boulders where no vegetation can grow), we can write:

$$\rho_1(t) + \rho_2(t) = 1 \qquad \text{(A1)}$$

Let us assume that community C_1 is occupying the left side of the lattice, community C_2 the right side, and the vegetation boundary is in between. Further, we define the positive x-direction to go from left to right. Then, the x-location of the optimal vegetation boundary at time t can be written more formally as:

$$B_{OPTIMAL} = \frac{Z\rho_1(t)}{L_Y} = L_X \rho_1(t) \qquad \text{(A2)}$$

In which $B_{OPTIMAL}$ indicates the x-coordinate of the optimal vegetation boundary position. From equations A1 and A2 it follows that the position of the optimal boundary changes over time as:

$$\frac{dB_{OPTIMAL}}{dt} = \frac{d\rho_1(t)}{dt} = -\frac{d\rho_2(t)}{dt} \qquad \text{(A3)}$$

Appendix 2: Derivation of the formation rate of retreating plant community 'islands'

In this Appendix, we provide a more detailed derivation of Equation 2 in the main text. Again we consider a community C_1 which is replacing community C_2, following a unidirectional version of the Eden model (e.g. Barabási and Stanley 1995). The rate of island formation is determined by two properties; 1) How far away from the previous C_1 frontrunner the new C_1 frontrunner colonizes a cell. 2) The number of cells in between the current and the new frontrunner that also become colonized by C_1 individuals in this timestep. Since the current C_1 frontrunner has a maximum dispersal distance of n cells, we need to consider colonization dynamics of the n cells in front of the current frontrunner. Generalizing the result shown in equation 1 in the main text, the probability of k cells getting colonized the next timestep is the product of the probability of k colonization events, p^k, and the probability of n-k cells not getting colonized, $(1-p)^{n-k}$. Thus, we can write:

$$P(k) = (1-p)^{n-k}\, p^k \qquad \text{(A4)}$$

In which $P(k)$ is the probability of k colonization events ahead of the current frontrunner. Now, we use j to indicate the number of cells between the new frontrunner and the current frontrunner of the C_1 community. If the establishment of this new frontrunner comprises the only colonization event of the timestep (k=1), then all the C_2 individuals in between the new frontrunner and the current frontrunner (j-1) become islands in the vegetation boundary. Thus, the number of islands formed depends on the advance of the frontrunner (j) and the total number of colonization events ahead of the previous frontrunner (k), yielding:

$$I(j,k) = j - k \,. \qquad \text{(A5)}$$

In which *I(j,k)* is the number of islands formed, given that the new frontrunner establishes *j* cells ahead of the current frontrunner, and in total *k* cells ahead of the current frontrunner getting colonized.

The average number of islands formed is then given by the product of the probability of an event (equation A4), and the number of islands that would be formed due to this event (equation A5) summed over all possible events. Taking into account that islands form as soon as $j>1$ and $j-1 \geq k$, this summation yields:

$$\sum_{j=2}^{n}\sum_{k=1}^{j-1} P(k)I(j,k) = \sum_{j=2}^{n}\sum_{k=1}^{j-1} (1-p)^{n-k}\, p^{k}\,(j-k) \qquad \text{(A6)}$$

Equation A6, however, underestimates the total number of islands formed, because multiplicity is not included in the equation. Multiplicity means that the same macrostate (i.e. the number of colonized and not colonized cells) can be achieved through multiple microstates (i.e. the specific state, colonized or not colonized, of each of the *n* cells). For example, when we consider a neighborhood of $n=5$ cells. In case of one colonization event, there are 5 possible configurations to achieve this (namely each of the 5 cells can be the one that is being colonized). In case of two colonization events, there are 4 possibilities left for the second colonization event. Because cells can be picked in any order, there are two ways to select the same pair of cells: either cell can be the one that is picked first. Thus, the total number of configurations is then $\frac{5*4}{2}$. Similarly in case of three colonization events, there will be 3 choices left for the third colonization event. Because the triplets can be picked in

any order, there are six ways to select the same triplet: each of the three cells can be picked first, and for each pick there are two ways to select the remaining pair of cells. Thus, the total number of configurations is then $\frac{5*4*3}{3*2}$. These examples indicate that we can generalize this result as:

$$\Omega(n,k) = \frac{n(n-1)(n-2),...,(n-k+1)}{k!} \qquad \text{(A7)}$$

In which $\Omega(n,k)$ gives the total number of spatial configurations (microstates) that yield the same macrostate of *k* colonization events within the *n* cells ahead of the current frontrunner. Using:

$$n(n-1)(n-2),...,(n-k+1) = \frac{n!}{(n-k)!} \qquad \text{(A8)}$$

We can write:

$$\Omega(n,k) = \frac{n!}{k!(n-k)!} \qquad \text{(A9)}$$

Equation A9 is the general multiplicity factor that is well known in statistical physics (e.g. Schroeder 2000). For our current model, however, we need to constrain the multiplicity factor. More specifically, one of the colonization events comprises the establishment of the new frontrunner, and its position *j* is constrained. The multiplicity factor therefore only applies to the *j*-1 cells in between the current and the new frontrunner, and to the colonization events additional to the new frontrunner

colonization (thus the remaining k-1 events). Substituting j-1 for n and k-1 for k in equation A9 then yields:

$$\Omega(j,k) = \frac{(j-1)!}{(k-1)!((j-1)-(k-1))!} = \frac{(j-1)!}{(k-1)!(j-k)!} \quad \text{(A10)}$$

Thus, in summary, the rate of island formation, F_2, is given by the product of three components: 1) The probability of k colonization events (the macrostate), 2) the number of islands that is formed due to these events 3) the multiplicity of the macrostate, i.e. the number of spatial configurations through which these events can be achieved. In equation form, this becomes:

$$F_2 = P(k)I(j,k)\Omega(j,k) = \sum_{j=2}^{n}\sum_{k=1}^{j-1}(1-p)^{n-k}\,p^k\,(j-k)\frac{(j-1)!}{(k-1)!(j-k)!} \quad \text{(A11)}$$

As presented in the main text (equation 2).

References

Barabási, H-L, and Stanley, H.E. 1995. Fractal concepts in surface growth. - Cambridge University Press.

Schroeder, D.V. 2000. An introduction to thermal physics. - Addison-Wesley.

Appendix 3: Additional model simulations and power analyses

In this Appendix, we report additional simulations using parameter variations and alternative functional forms of the model presented in the main text. We also perform power analyses on images generated by model simulations. Finally, we examine the effect of environmental fluctuations on the accuracy of the method

Effect of differences in competitiveness on boundary movement

We first focused on the effect of the strength of competition on distances of community fronts to the optimal boundary. Focusing on a situation of competitive exclusion, simulations show that the larger the difference in competitiveness, the faster the superior competitor expands (and the boundary moves, Fig. A1a). This result is consistent with previous results from a different model (O'Malley et al. 2009). Further, vegetation boundary movement increases with the size of the interaction neighborhood (Fig. A1a). The types of interaction neighborhoods considered are listed in Table A1. In the main text, we noted that the front of the expanding community is distinctly closer to the optimal boundary position than the retreating community at any particular moment in time. This result does not depend on specific assumptions about the interaction neighborhood. The same result occurs when the expanding community has a much smaller (Fig. A1b) or much larger (Fig. A1c) interaction neighborhood than the retreating community. Differences in interspecific competition have little effect on the variation in community front positions, meaning that the required number of observations to achieve satisfactory power is similar for different interspecific competition settings (Fig. A1d). This issue is further treated in the power analyses section of this Appendix.

Effect of ecosystem feedbacks on boundary movement

The model of Eppstein and Molofsky (2007) enables the inclusion of feedbacks between the two communities, via the species interaction feedback coefficients $\alpha_{11,}$ $\alpha_{12,}$ $\alpha_{21,}$ and α_{22}. Both empirical and theoretical studies suggest that feedbacks may be crucial for the outcome of plant competition and species invasion (Bever et al. 1997; Klironomos 2002). Whether the rate of spread of expanding species is affected by feedbacks, however, is less clear (Levine et al. 2006; Eppstein and Molofsky 2007). We further address this latter question by studying the effect of different feedback combinations on the rate of spread of expanding plant communities. Although previous studies have shown that strong feedbacks can even alter the outcome of competition qualitatively (Eppinga et al. 2006), we focus here on a situation where the competitively superior community outcompetes another community, but at different rates due to net interaction feedback (i.e. $\alpha_{11} - \alpha_{12} - \alpha_{21} + \alpha_{22}$, Bever et al. 1997) within the system. If within-community feedbacks are stronger than between-community feedbacks, there is a net positive feedback in the system (Bever et al. 1997). If between-community feedbacks are stronger than within-community feedbacks, there is a net negative feedback in the system (Bever et al. 1997).

The movement of the expanding front is slightly accelerated under negative feedback, but it is slowed under strong positive feedback (Fig. A2a). Negative feedback enhances the possibility of both communities to expand into the area dominated by the other community. Strong positive feedback creates Allee-like effects (Hastings et al. 2005; Takimoto 2009), meaning that small patches of either community are often rapidly replaced. This may be accompanied by a decrease in variation in front positions, depending on the interaction neighborhoods of the two communities. As a result, the required number of observations to achieve satisfactory power would decrease (Fig. A2c). This issue is further treated in the power analyses section below.

Power analyses

In this section we examine under which conditions differences in distance to the optimal boundary become more difficult to detect, and thus call for a relatively large number of observations in the image. The required number of observations for a preset effect size (i.e. difference in boundary positions) depends on the variation in the observed difference between frontrunners of both communities. As mentioned earlier, this variation is little influenced by interspecific competition settings (Fig. A1d). Instead, the degree of variation is influenced by the size of the interaction neighborhoods of the two plant communities. In general, larger interaction neighborhoods lead to community fronts with larger variation. This suggests that predictions about the movement of such vegetation boundaries should consist of a higher number of observations to achieve satisfactory power (Fig. A1d).

Interestingly, strong positive feedback may reduce the amount of variation within community front positions, because relatively disorganized patches rapidly disappear (Fig. A2c). However, positive feedback may also slow the invasion process (Fig. A2a), making it more dependent on stochastic events that could increase variation. Hence, the effect of positive feedback on the required number of observations to achieve satisfactory power is context dependent (Fig. A2c).

The effect of environmental fluctuations

In the above simulations, competition coefficients were kept constant during the simulations. Due to environmental fluctuations, however, the competitiveness of communities may vary over time. We mimicked environmental fluctuations by putting stochastic noise on competition coefficients, so that the values of these coefficients changed each timestep. The mean values of the competition coefficients were set in a way that lead to competitive exclusion in the absence of fluctuations.

Figure A3 shows the correspondence between the current difference between the two communities in their distance to the optimal vegetation boundary, and past boundary movement. Without environmental fluctuations, the vegetation boundary analysis not only accurately reflects boundary movement over longer time periods (Fig. A3b), but it also corresponds well to movement that occurred in the most recent timestep (Fig. A3a). This can be explained by the fact that boundary movement is relatively constant in the absence of environmental fluctuations. When fluctuations are included, however, the vegetation boundary analysis only accurately reflects boundary movement over longer time periods (Fig. A3c,d). This means that the vegetation boundary is not strongly responding to changes over a single timestep (i.e. year-to-year variation), but it reflects competitive interactions over longer periods of time. This observation has consequences for the utility of the method to be used as a predictor for future boundary dynamics (Fig. A4). In the absence of environmental fluctuations, the analysis provides an accurate prediction for both the next timestep and for the dynamics over longer periods of time (Fig. A4a,b). When environmental fluctuations are included, however, only the boundary dynamics over a longer term are still relatively accurately (< 3% incorrect) predicted (Fig. A4c,d).

To address the question whether the boundary analysis can be applied to systems that are subject to effects related to global change, we performed an additional simulation. In this simulation, competition coefficients were set in a way that lead to a stable vegetation boundary for the first 500 timesteps. Then, the interspecific competition coefficient for one community gradually decreased, mimicking increasing competitiveness (e.g. due to changing climatic conditions). Environmental fluctuations were included in this simulation as well. As a result of the gradual change, the vegetation boundary moved with an accelerating rate (Fig. A5a). It is important to note that despite the fact that vegetation boundary dynamics do not respond that strongly to year-to-year changes, the vegetation boundary analysis

230 detects changing dynamics due to a long-term trend in environmental conditions
231 relatively rapidly (A5b).
232

233 References

234 Bever, J.D. et al. 1997. Incorporating the soil community in plant population
235 dynamics: the utility of the feedback approach. – J. Ecol. 85: 561-573.
236 Eppinga, M.B. et al. 2006. Accumulation of local pathogens: a new hypothesis to
237 explain exotic plant invasion. - Oikos 114: 168-176.
238 Eppstein, M.J. and Molofsky, J. 2007. Invasiveness in plant communities with
239 feedbacks. – Ecol. Lett. 10: 253-263.
240 Hastings, A. et al. 2005. The spatial spread of invasions: new developments in theory
241 and evidence. – Ecol. Lett. 8: 91-101.
242 Klironomos, J.N. 2002. Feedback with soil biota contributes to plant rarity and
243 invasiveness in communities. - Nature 417: 67-70.
244 Levine, J.M. et al. 2006. Plant-soil feedbacks and invasive spread. – Ecol. Lett. 9:
245 1005-1014.
246 O'Malley, L. et al. 2009. Ecological invasion, roughened fronts, and a competitor's
247 extreme advance: integrating stochastic spatial-growth models. – Bull. Math. Biol.
248 71: 1160-1178.
249 Takimoto, G. 2009. Early warning signals of demographic regime shifts in invading
250 populations. – Popul. Ecol. 51: 419-426.

251 Figure A1

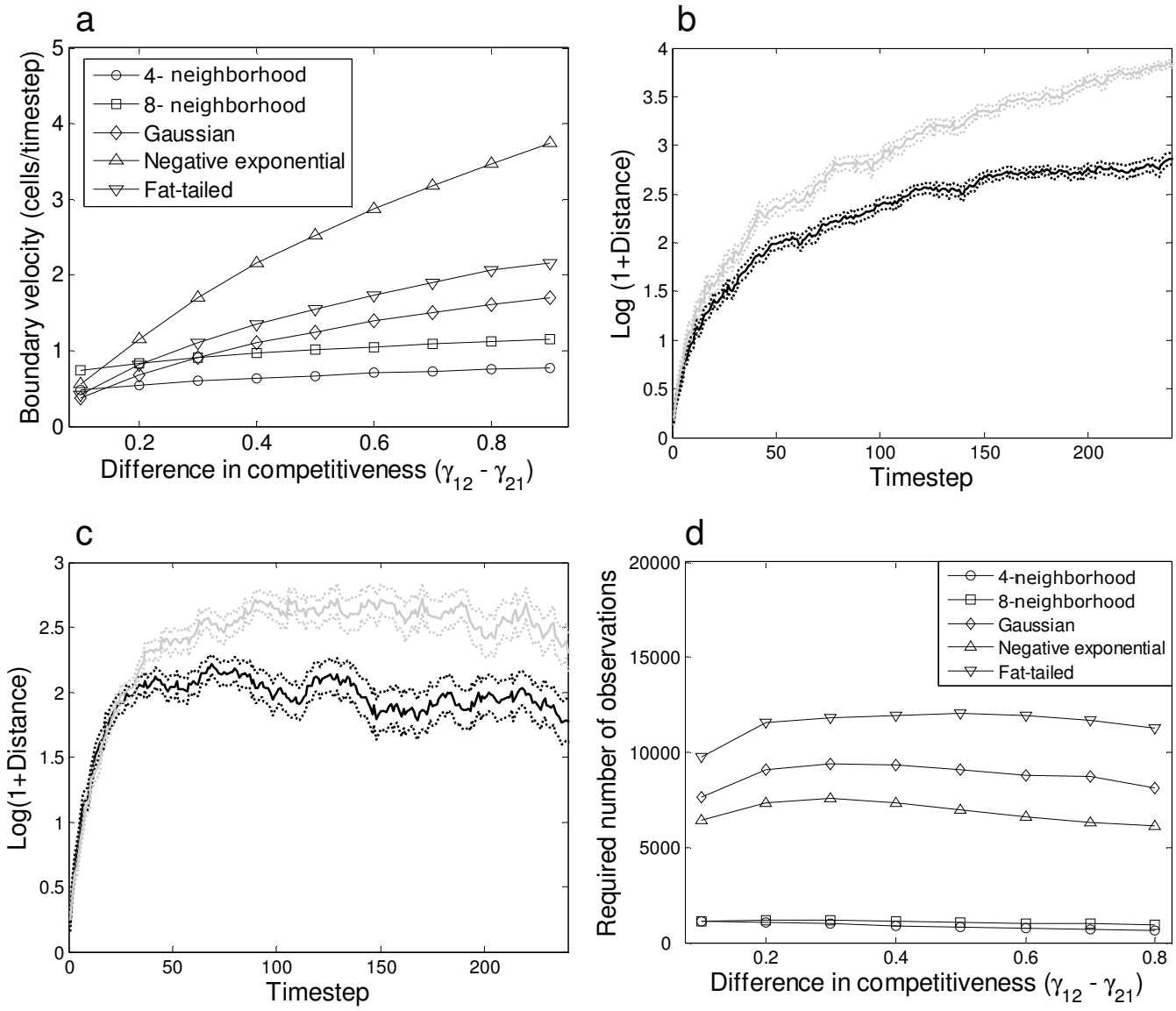

Figure A1: Model simulations examining the effect of interspecific competition on vegetation boundary propagation, for different sizes of interaction neighborhoods. Each symbol represents the average of 10 simulations. a) The vegetation boundary propagation velocity increases with decreasing amount of interspecific competition experienced by the expanding community. b) The boundary position of the expanding community (black line) is consistently closer to the optimal boundary than that of the retreating community (gray line), also when the interaction neighborhood of the expanding community (8 nearest neighbors) is much smaller than that of the retreating community (negative exponential kernel). c) The boundary position of the expanding community (black line) is also closer to the optimal boundary than that of the retreating community (gray line) when the interaction neighborhood of the expanding community (negative exponential kernel) is much larger than that of the retreating community (8 nearest neighbors). d) Power analyses revealing the number of observations needed to be able to detect a distance between transformed vegetation boundary positions of 0.2. In general, vegetation boundaries involving communities with larger interaction neighborhoods require a larger number of observations. Parameter values (see main text and Table A1) were set as follows: $b=0$, $d_1 = d_2=0.1$, $\beta_1= \beta_2=1$, $K_1= K_2=1$, $\gamma_{11}= \gamma_{22}=1$, $\gamma_{12}= 1$, $\gamma_{21}=0.1\text{-}0.9$, $w=2$, $L=5$, $\alpha=2$. Model lattices consisted of 256*256 cells (a,d) or 1024*1024 cells (b, c), respectively.

Figure A2

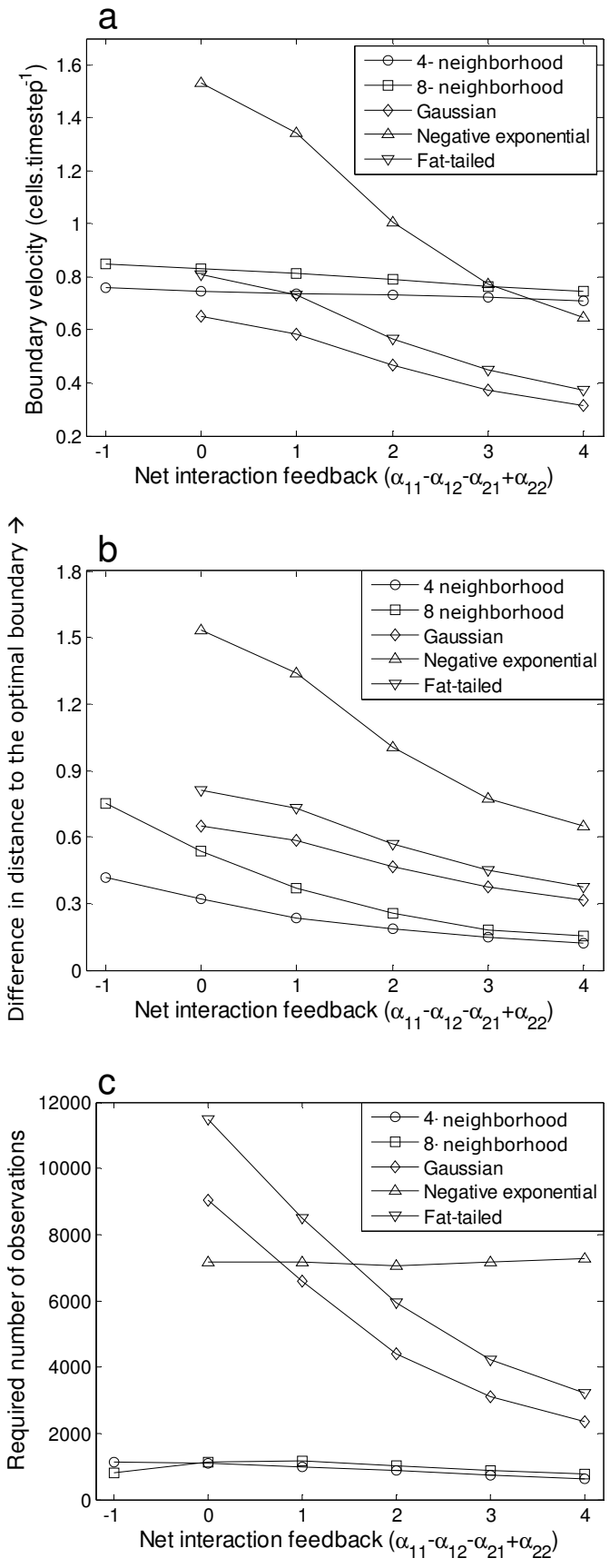
a
Boundary velocity (cells.timestep-1)
4- neighborhood
8- neighborhood
Gaussian
Negative exponential
Fat-tailed
Net interaction feedback (α11-α12-α21+α22)
b
Difference in distance to the optimal boundary →
4 neighborhood
8 neighborhood
Gaussian
Negative exponential
Fat-tailed
Net interaction feedback (α11-α12-α21+α22)
c
Required number of observations
4· neighborhood
8· neighborhood
Gaussian
Negative exponential
Fat-tailed
Net interaction feedback (α11-α12-α21+α22)

Figure A2: Model simulations examining the effect of positive and negative feedbacks on vegetation boundary propagation, for different sizes of interaction neighborhoods. Each symbol represents the average of 30 simulations. a) The vegetation boundary propagation velocity decreases when feedback increases from negative to strongly positive. b) Also, the difference in distance to the optimal vegetation boundary between the two communities decreases when feedback increases from negative to strongly positive. c) The number of observations needed to gain an image with satisfactory power is largest for intermediate magnitude of positive feedback. A net interaction feedback of -1 was achieved by setting by α_{11}=-0.25, α_{12}=0.25, α_{21}=0.25, α_{22}=-0.25. Adding 0.25 to each feedback interaction coefficient then increased the net interaction feedback by 1. Other parameters as in Figure A1. Model lattices consisted of 256*256 cells

299 Figure A3

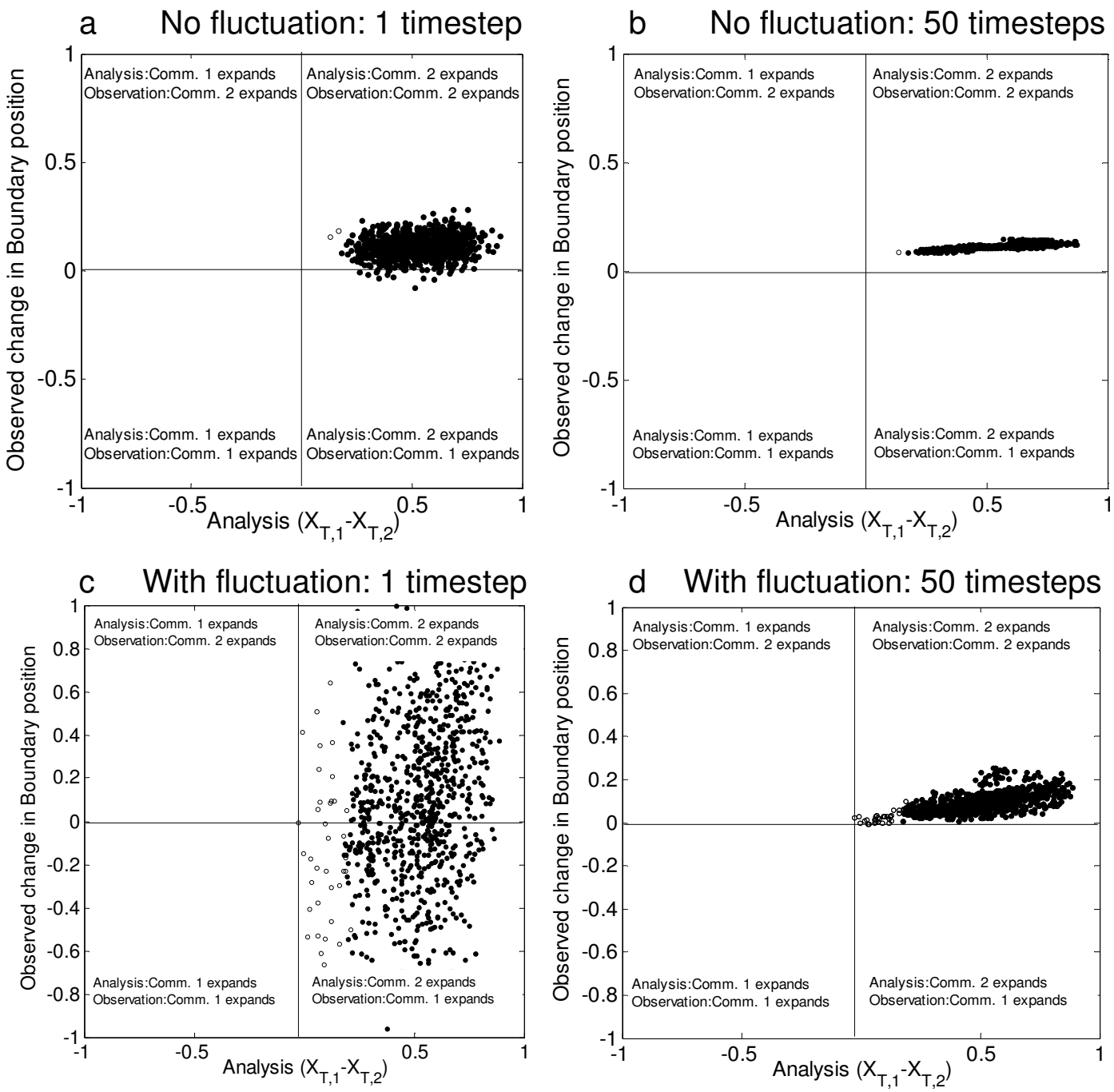

Figure A3: Model simulations examining the effect of environmental fluctuations on the accuracy of the method reflecting past boundary dynamics. For each timestep, the boundary analyses is performed and compared to the actual boundary movement during the last timestep or the last 50 timesteps of the simulation. Open symbols represent timesteps where the analysis yielded no conclusion due to lack of sufficient power. Closed symbols represent conclusions based on the analysis. Note that symbols situated in the first and third quadrants represent correct conclusions (i.e. consistent with the observation), whereas symbols situated in the second and fourth quadrants represent incorrect conclusions. a-b) When no fluctuations are included, the boundary analysis accurately reflects both short-term and long-term boundary movement. c-d) When fluctuations are included, the boundary analysis only reflects long-term boundary movement accurately. Competition effects were set as follows: $\gamma_{11}= \gamma_{22}=1$, $\gamma_{12}= 1$, $\gamma_{21}=0.9$, environmental fluctuation was included by adding each timestep a randomly drawn quantity between -0.375 to + 0.375 to the baseline values of γ_{12} and γ_{12} as noted above. Other parameters as in Figure A1. Simulations were run for 1000 timesteps, and analyzed after an initialization period of 150 timesteps. Model lattices consisted of 1024*1024 cells and considered a 4 nearest neighbors interaction neighborhood.

318 Figure A4

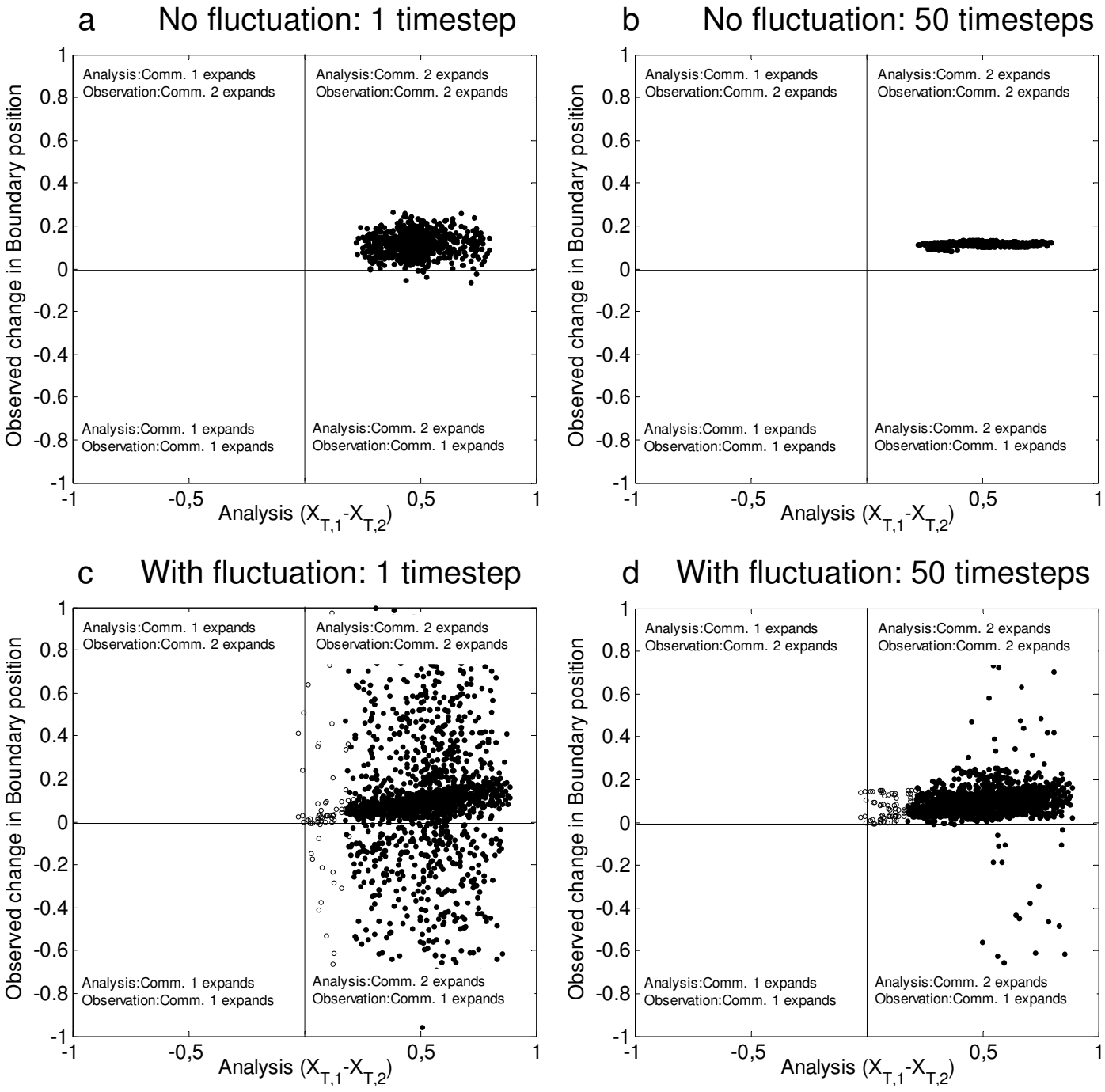

Figure A4: Model simulations examining the effect of environmental fluctuations on the accuracy of the method predicting future boundary dynamics. For each timestep, the boundary analyses is performed and compared to the actual boundary movement that occurred in the next timestep or the average movement that occurred in the next 50 timesteps of the simulation. Open symbols represent timesteps where the analysis yielded no prediction due to lack of sufficient power. Closed symbols represent prediction based on the analysis. Note that symbols situated in the first and third quadrants represent correct predictions (i.e. consistent with the observation), whereas symbols situated in the second and fourth quadrants represent incorrect predictions. a-b) When no fluctuations are included, the boundary analysis accurately predicted both short-term (1 timestep) and long-term (50 timesteps) future boundary movement. c-d) When fluctuations are included, the boundary analysis only predicts long-term boundary movement accurately. Parameters and model specifications were set as in the same way as in Figure A3.

333 Figure A5

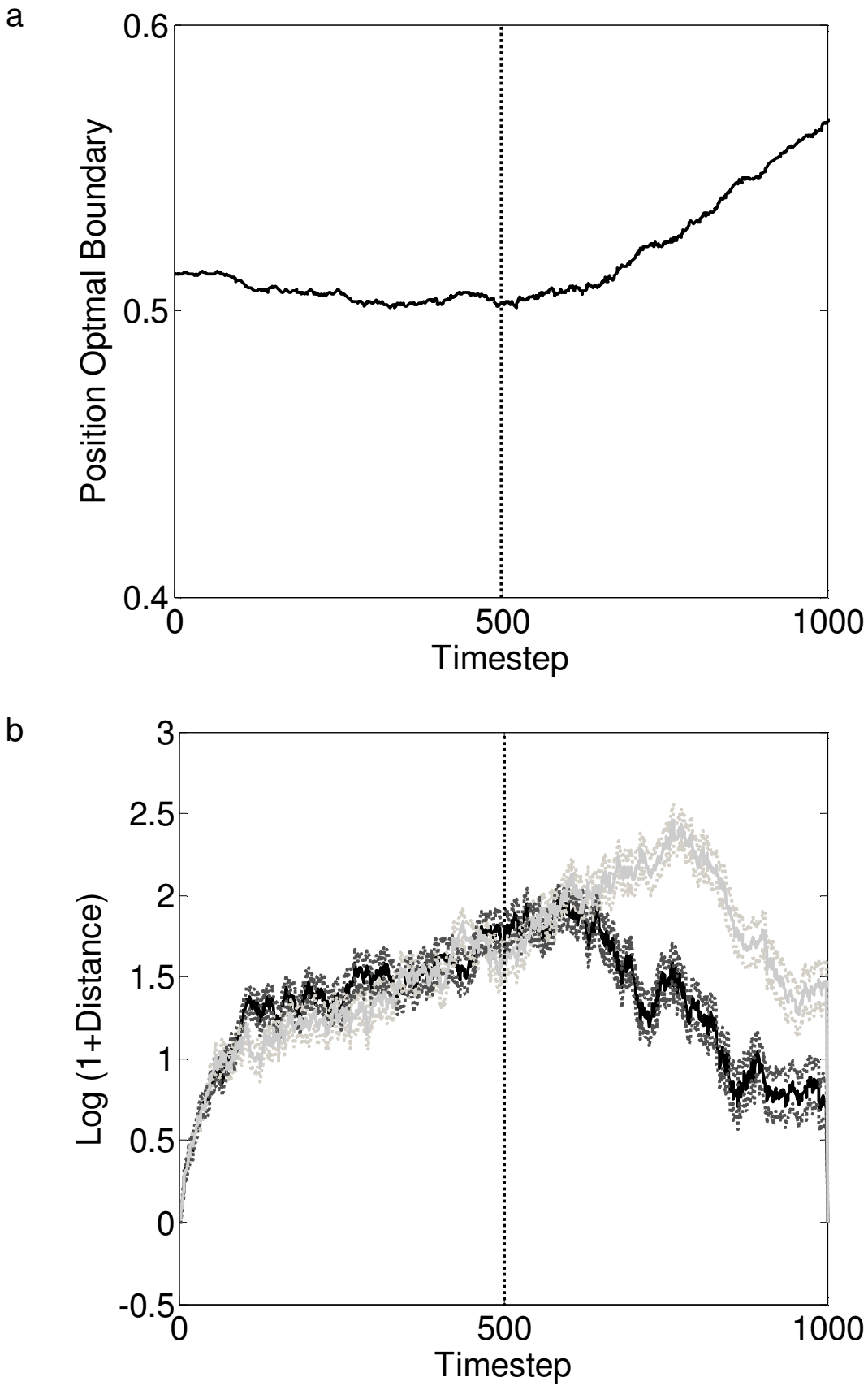

Figure A5: Model simulations examining the effect of environmental fluctuations on detecting changes in the boundary dynamics due to environmental change. a) Due to a gradual change in environmental conditions that starts after 500 timesteps, the vegetation boundary becomes unstable, and one vegetation community begins to expand. b) Despite environmental fluctuations affecting the vegetation boundary dynamics, the change in environmental conditions and the resulting change in community abundances is detected relatively rapidly. During the first 500 timesteps of the simulation, competition coefficients were set as follows: γ_{12}= 1, γ_{21}=1. From that point onward, there was a linear decrease in γ_{21}, which reached a value of 0.8 at the end of the simulation (after 1000 timesteps). Other parameters and model specifications were set as in the same way as in Figure A3.

Table

Table A1: The characteristics of the interaction neighborhoods and the model parameters used in this appendix.

Type of neighborhood	**Description of neighborhood**
4-neighborhood (discrete)	The cells adjacent to the edges
8-neighborhood (discrete)	All directly surrounding cells
Gaussian kernel	$\int_{\Omega} \frac{1}{\sqrt{2\pi w^2}} e^{-\frac{\lvert x-y \rvert}{2w^2}} dy$
Negative exponential kernel	$\int_{\Omega} \frac{1}{2L^2} e^{-\frac{2\lvert x-y \rvert}{L}} dy$
Fat-tailed kernel	$\int_{\Omega} \frac{1}{4\alpha} e^{-\sqrt{\frac{\lvert x-y \rvert}{\alpha}}} dy$

Appendix 4: Image processing details

In this Appendix we explain the image processing procedure that was followed to obtain the images shown in Figures 4 and 5 of the main text.

Northern hardwood–boreal forest ecotone in Vermont (Camels Hump)

The image used in the vegetation boundary analysis of Camels Hump was a 2005 multi-spectral Quickbird satellite image (Satellite Imaging Corporation, Houston, TX), which we classified using the ERDAS IMAGINE 8.7 image processing software package (Leica Geosystems, 2005). The image captures the entire boreal forest found on Camels Hump and extends below the northern hardwood forest, possibly including riparian areas containing the low elevation conifer *Tsuga Canadensis* (eastern hemlock). In order to avoid the classification of hemlock, which does not extend into the ecotonal region, elevations below 650m were masked out prior to image analysis using a digital elevation model. Sub-pixel influences such as tree shadows were reduced by smoothing each of the satellite image bands (panchromatic [grayscale], red, green, blue and near-infrared) using a low-pass 5X5 pixel filter. In addition to the panchromatic and multi-spectral image layers, we created three commonly used index layers designed to enhance classification: a normalized difference vegetation index (NDVI) layer, an infrared to red (IR:R) ratio layer, and a texture layer. The goal of the NDVI and the IR:R ratio is to reduce misclassification by enhancing the differences between vegetation types in photosynthetically active wavelengths that have been found to be useful in forest community discrimination (near infrared and red, Tucker 1979; Pettorelli et al. 2005). A texture layer was also used for classification to take advantage of the inherent differences in the shape of a hardwood versus a coniferous canopy since a deciduous hardwood canopy would appear much smoother than that of a coniferous one (Franklin et al. 2000). These indices have the added benefit of

374 reducing the impact of shadows on image classification (Puissant et al. 2005). These
375 eight layers were then put through an unsupervised classification procedure. In
376 IMAGINE this classification procedure utilizes an iterative clustering technique based
377 on Euclidean spectral distances called the Iterative Self-Organizing Data Analysis
378 Technique (ISODATA) commonly used for multispectral imagery (Leica Geosystems
379 2007, Richards 1993). We used ISODATA clustering to generate 25 classes from a
380 maximum of 50 iterations and a convergence threshold of 95%, which allows a
381 solution to be reached when 95% of the pixels remain in the same cluster between
382 iterations. Using a small subset of the original satellite image, these classes were then
383 visually identified as bare rock or assigned to either boreal or hardwood forest classes
384 (Fig. A6), leading to the three-class image presented in the main text.
385 It is important to note that the presence of pixels of the third image class
386 (boulder or *Tsuga canadensis*) did not affect the outcome of the vegetation boundary
387 analysis. This could be achieved by ignoring these cells in the calculation of the
388 optimal boundary position and in the calculation of frontrunner distances. In practice,
389 this meant that the lattice was no longer a perfect grid, but there were holes in the grid
390 that could not be occupied by the northern hardwood community or the boreal forest
391 community.
392
393 **Forest-mire ecotone in New Zealand**
394 The image used in the vegetation boundary analysis of the pakihi system in New
395 Zealand was imported as a screenshot from Google Earth into the Matlab
396 programming environment (v. 2006a, Mathworks, 2006). The color image was then
397 decomposed into red, green and blue layers ranging between 0 (color not present) and
398 255 (color entirely present). Again, sub-pixel influences such as tree shadows were
399 reduced by smoothing the red, green and blue layers using a low-pass 5X5 pixel filter.
400 Forest community pixels had a higher proportion of green and blue color, which was

401 used in the classification procedure. More specifically, pixels that consisted for more
402 than 2/3 of green and blue colors were classified as forest community, other pixels as
403 mire community. The smoothing filter described above did not erase a few multi-pixel
404 (but still relatively small) patches of shadow within the forest community, which were
405 then incorrectly classified as mire community. Therefore, mire community pixels that
406 were within the forest community (within 125 pixels of the right end of the picture)
407 and were part of a relatively small patch (clump of pixels smaller than 200), were
408 changed into forest community pixels. This resulted in the two-class image presented
409 in the main text.
410

411 ## References

412 Franklin, S.E. et al. 2000. Incorporating texture into classification of forest species
413 composition from airborne multispectral images. – Int.. J. Rem. Sens. 21: 61-
414 79.
415 Pettorelli, N. et al. 2005. Using the satellite derived NDVI to assess ecological
416 responses to environmental change. – Trends Ecol. Evol. 20: 503-510.
417 Puissant, A. et al. 2005. The utility of texture analysis to improve per-pixel
418 classification for high to very high spatial resolution imagery. – Int. J. Rem.
419 Sens. 26: 733-745.
420 Tucker, C.J. 1979. Red and photographic infrared linear combinations for monitoring
421 vegetation. – Rem. Sens. Env. 8: 127-150.

422

Figure A6

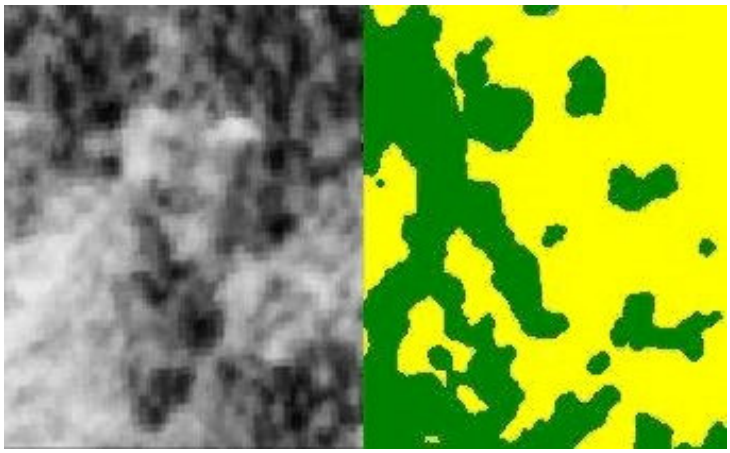

Figure A6: An example of forest class designations overlaid on a subset of the original panchromatic satellite image.

Appendix 5: Density profiles of vegetation communities

In this Appendix we present the density profiles of the vegetation boundaries that are presented in the section Application to Earth Observation derived boundary maps of the main text.

As suggested in the main text, the distance to the optimal boundary position can be used to predict boundary movement. In addition, the density profiles may indicate about whether the retreating community is disappearing entirely or not. In general, the six frames on Camels hump have a declining density profile, although the trend is not as clear as in model simulations (Fig. A7). The occurrence of local maxima in the density profile could indicate the presence of satellite populations (Moody and Mack 1988). If satellite populations are present, the distance to the optimal boundary becomes a less reliable indicator for boundary movement. Closer inspection of the frames within the larger figure (Fig. 4 in the main text), however, does not suggest a spreading pattern from satellite populations but a single front following the mountain contours. Moreover, the deviations from the trends in the density profile are relatively small (Fig A7). This would suggest that the hardwood community is replacing the boreal forest community rather than a mixing of the two communities. However, our results are in compliance with the original study by Beckage et al. (2008), who noted that total exclusion of boreal species at lower elevations has not yet been observed. Hence, the possibility of a mixing boundary cannot yet be ruled out.

The forest-mire ecotone in New Zealand clearly shows a consistent trend in the density profile (Fig. A8). Together with the observation that both community fronts are at similar distance to the optimal boundary (see main text), this suggests that the vegetation boundary is stable.

The density profile of the field data snapshot of the subalpine treeline-tundra ecotone shows a declining trend in tree density, until it becomes more constant at low density (Fig. A9). Interestingly, the two snapshots from a model simulation show different density profiles. This suggests that a community front may not be advancing at a constant rate (Zeng and Malanson 2006). The first snapshot shows a distinct zone of relatively constant density, which occurs in our model simulations of mixing boundaries (see main text). Some mixing may indeed occur in the subalpine treeline-tundra system: tree patches can advance (relatively rapidly) and tundra may establish in small patches of uniform tree cover that are in front of the average boundary position and become limited by resources (Zeng and Malanson 2006). In large patches with high density of trees (lower than uniform tree cover), however, tundra is not expanding, meaning that mixing throughout the entire lattice does not occur. In the second snapshot, the vegetation boundary is much sharper, as represented by a consistent trend in the density profile (Fig. A9). Together with the closer distance of the alpine treeline community to the optimal vegetation boundary, this suggests the alpine treeline community replacing the tundra community.

A clear difference between the Earth Observation derived snapshot and the model simulation snapshots are the density profiles toward the edge of the image. The model simulations have converged to relatively constant values (Fig. A9). Therefore, an analysis of community front strength is not affected by selecting a slightly smaller or larger image. On the contrary, the density profile of the field snapshot has not stabilized yet at the edges of the image (Fig. A9). Therefore, taking a slightly larger image may yield a different result of the vegetation boundary analysis. In the main text, a subset of a model simulation is taken, which mimics the density profile as observed in the field data snapshot (Fig. A9). As shown in the main text, the smaller image indeed yields a different prediction on vegetation boundary movement.

References

Beckage, B. et al. 2008. A rapid upward shift a forest ecotone during 40 years of warming in the Green Mountains of Vermont. – Proc. Natl Acad. Sci. USA 105: 4197-4202.

Moody, M.E. and Mack, R.N. 1988. Controlling the spread of plant invasions: the importance of nascent foci. – J. Appl. Ecol. 25: 1009-1021.

Zeng, Y. and Malanson, G.P. 2006. Endogenous fractal dynamics at alpine treeline ecotones. – Geogr. Anal. 38: 271-287.

Figure A7

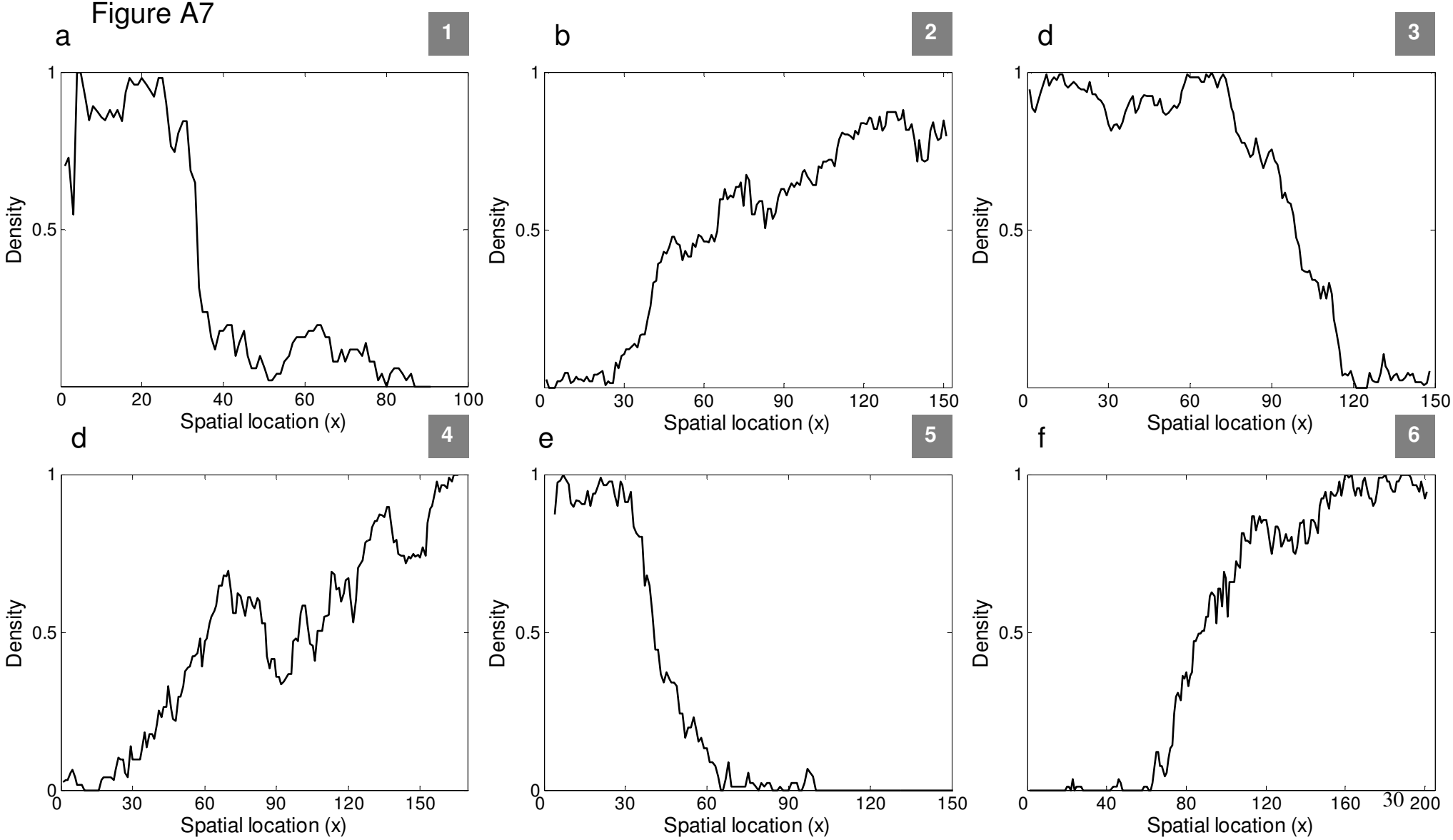
a
1
b
2
d
3
d
4
e
5
f
6
Density
Spatial location (x)
0
0.5
1
0
20
40
60
80
100
30
90
120
150
160
200

Figure A7: Density profiles of the snapshots taken from the northern hardwood-boreal forest ecotone on Camels Hump (Vermont). The density profile is given as the fraction of vegetated cells that is occupied by the northern hardwood community along the elevation gradient.

Figure A8

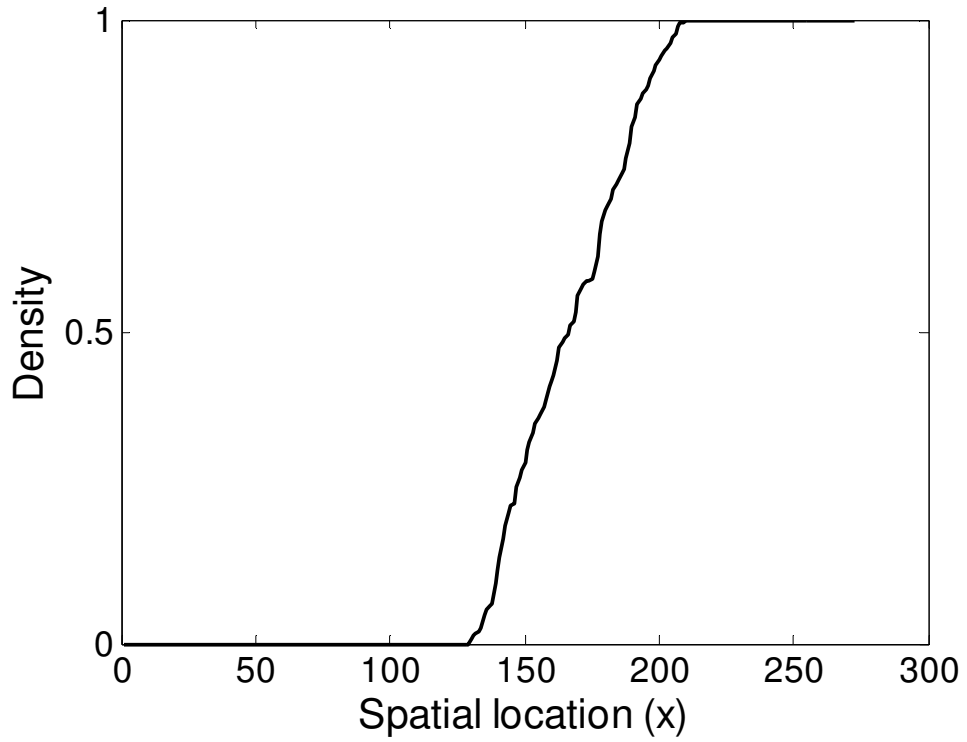

Figure A8: Density profile of a snapshot of a forest-mire ecotone in New Zealand. The density profile is given as the fraction of vegetated cells that is occupied by the forest community.

1 Figure A9

2

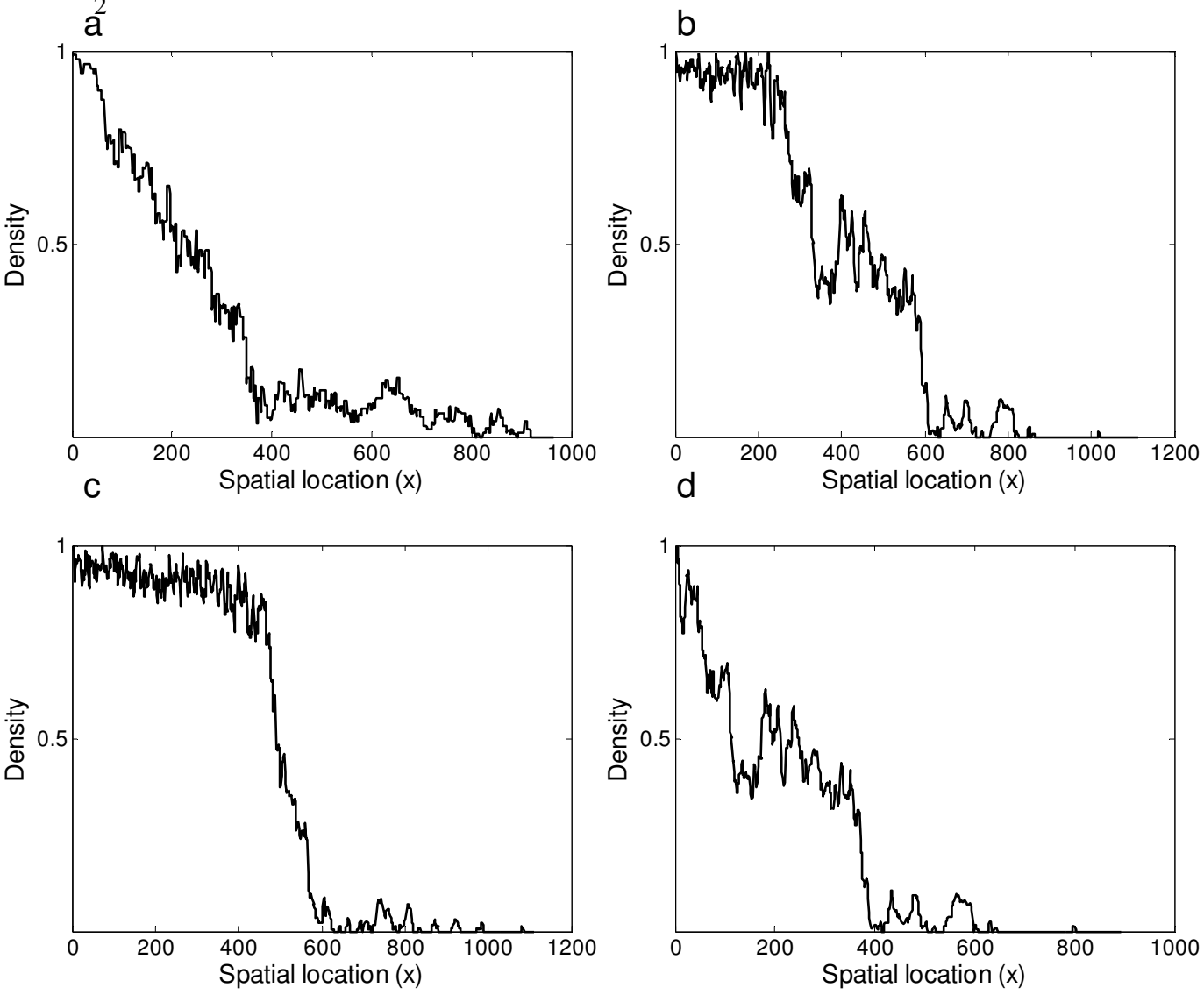

Figure A9: Density profiles of the snapshots of model simulations and an ADAR image (from Zeng and Malanson 2006) of a subalpine treeline-tundra ecotone in Glacier National Park, Montana. The density profile is given as the fraction of vegetated cells that is occupied by the alpine treeline community.